SAND2021-10205C

Spectral Equivalence Properties of Higher-Order Tensor Product Finite Elements

Clark R. Dohrmann

Abstract We present spectral equivalence results for higher-order tensor product edge-, face- and interior-based finite elements. In particular, we show for certain choices of shape functions that the mass and stiffness matrices of the higher-order elements are spectrally equivalent to those of an assembly of lowest-order elements on the associated Gauss-Lobatto-Legendre mesh. Using this equivalence, efficient domain decomposition or multigrid preconditioners can be designed which have favorable computational complexity. Numerical results are presented which confirm the spectral equivalence results.

1 Introduction

The focus of this study is on spectral equivalence results for higher-order tensor product finite elements in the $H(\text{curl})$, $H(\text{div})$, and L^2 function spaces. For certain choices of the higher-order shape functions, the resulting mass and stiffness matrices are spectrally equivalent to those for an assembly of lowest-order edge-, face- or interior-based elements on the associated Gauss-Lobatto-Legendre (GLL) mesh. This equivalence will help enable the development of efficient domain decomposition or multigrid preconditioners. Specifically, preconditioners for the equivalent lowest-order linear system can be used for the higher-order problem and avoid the demands of assembling a higher-order coefficient matrix.

Using assemblies of lowest-order (linear) elements for efficient preconditioning of higher-order discretizations in the function space H^1 is not new. We refer the interested reader to Section 7.1 of [10] or the introduction of [2] for a discussion of the pioneering work by Orszag [9], Deville and Mund [3, 8], Canuto [1] and others. We are, however, not aware of similar approaches for problems using higher-order edge- (Nédélec), face- (Raviart-Thomas) or interior-based elements. We note for the

Clark R. Dohrmann
Sandia National Laboratories, Albuquerque, New Mexico, USA, e-mail: crdohrm@sandia.gov

case of nodal elements that the degrees of freedom (DOFs) for a higher-order element and its equivalent assembly of lowest-order elements are nodal values in both cases. This natural one-to-one correspondence of DOFs can be realized for edge-, face- and interior-based elements by using shape functions (bases) associated with integrals and introduced by Gerritsma [5].

For edge-based elements, the DOFs for the shape functions are associated with integrals of tangential components of a vector field along each edge of the associated GLL mesh (see Figure 1 left). Similarly, DOFs for face-based elements correspond to integrals of the normal component of a vector field over individual faces of the GLL mesh (see Figure 1 right). For completeness, we also present shape functions and equivalence results for related interior-based elements. For these elements, the DOFs correspond to integrals of a scalar function over individual elements of the GLL mesh. We note in all three cases that the shape functions can be expressed simply in terms of one-dimensional interpolatory nodal functions at the GLL points along with a one-dimensional function which enables the correspondence between DOFs of the higher- and lowest-order elements.

The paper is organized as follows. Shape functions for edge-, face-, and interior-based elements are described in §2. This is followed in §3 by a presentation of spectral equivalence results between higher-order elements and their lowest-order counterparts. Numerical results are presented in §4 which confirm these results. A more comprehensive report [4] can be consulted for complete proofs and applications of the spectral equivalence results to preconditioning.

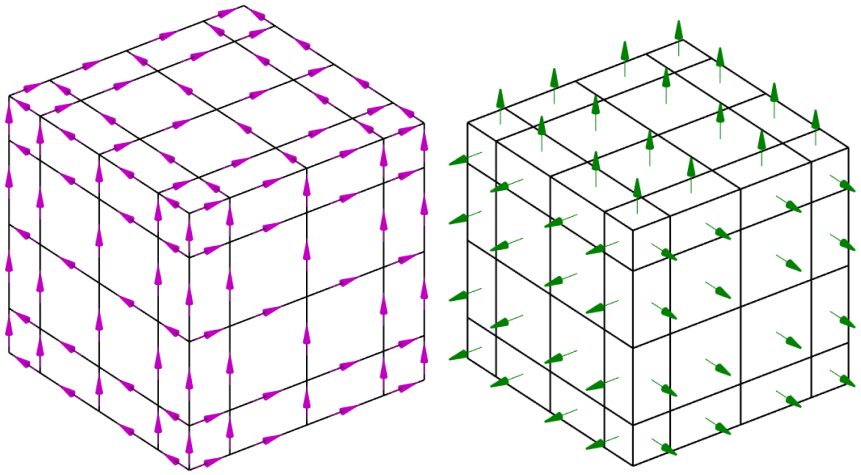

Fig. 1 Edge (left) and face (right) locations on three faces of a cube for a higher-order element of degree $p = 4$. Also shown is the corresponding assembly of p^3 lowest-order elements on the associated Gauss-Lobatto-Legendre (GLL) mesh.

2 Shape Functions

Following the notation in [7], let $Q_{i,j,k}$ denote the space of polynomials in reference element coordinates $(\eta_1, \eta_2, \eta_3) \in [-1, 1]$ for which the maximum degree is i in η_1, j in η_2 and k in η_3.

As is commonly done for nodal elements, one-dimensional GLL shape functions $\phi_0, \ldots, \phi_p$ are used to construct higher-order shape functions in three dimensions. See Figure 2 (left) for the case of degree $p = 4$. Notice that these functions are simply interpolatory (Lagrange) shape functions at the GLL points $x_0 = -1, x_p = 1$, and $x_{i-1} < x_i$ for $i = 1, \ldots, p$. We remark that the internal GLL points $x_1, \ldots, x_{p-1}$ are the roots of L'_{p-1}, where L_p is the Legendre polynomial of degree p.

Shape functions for edge-, face-, and interior-based elements based on the work of Gerritsma [5] are described next. Although different from the shape functions in [7], they span the same polynomial spaces and are conforming between elements.

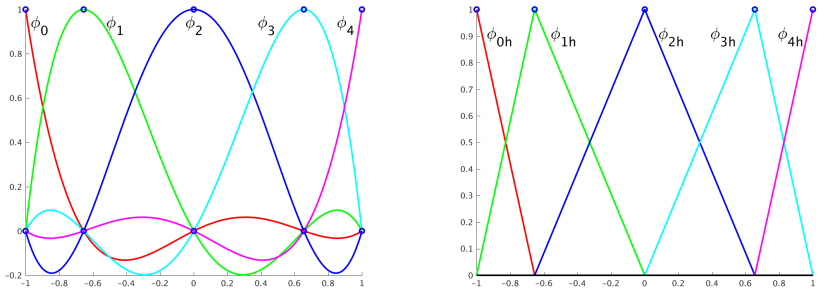

Fig. 2 One-dimensional higher-order (left) and linear (right) shape functions associated with GLL points for degree $p = 4$.

2.1 Edge Shape Functions

The vector field for an edge-based finite element of degree p can be expressed in terms of the reference element coordinates as

$$\boldsymbol{u}_p^{\mathrm{e}} = u_{1p}^{\mathrm{e}} \boldsymbol{b}_1 + u_{2p}^{\mathrm{e}} \boldsymbol{b}_2 + u_{3p}^{\mathrm{e}} \boldsymbol{b}_3,$$

where $u_{1p}^{\mathrm{e}} \in Q_{p-1,p,p}$, $u_{2p}^{\mathrm{e}} \in Q_{p,p-1,p}$, $u_{3p}^{\mathrm{e}} \in Q_{p,p,p-1}$, and $\boldsymbol{b}_1, \boldsymbol{b}_2, \boldsymbol{b}_3$ are unit vectors associated with the element coordinates (see e.g. [7]).

Our present focus is on edges aligned with the $\boldsymbol{b}_1$ direction; similar constructions of shape functions hold for edges aligned with the other two directions. For each $i \in \{0, \ldots, p-1\}$ define

$$\psi_i(\eta_1) = \sum_{m=0}^{p} a_{im}\phi_m(\eta_1), \qquad a_{im} = \begin{cases} 0 & m \le i \\ 1 & m > i \end{cases}$$

Since $\psi_i(x_{m+1}) - \psi_i(x_m)$ is 1 for $m = i$ and 0 for $m \neq i$, it follows that

$$\int_{x_m}^{x_{m+1}} \psi_i' \, dx = \delta_{im}, \tag{1}$$

where δ_{im} is the Kronecker delta function. The edge functions $\psi_0', \ldots, \psi_{p-1}'$ and their application to tensor product finite elements are discussed in [5].

Let $\mathcal{E}_{ijk}$ denote the edge with $\eta_1 \in (x_i, x_{i+1})$, $\eta_2 = x_j$ and $\eta_3 = x_k$. The shape function associated with this edge is given by

$$\boldsymbol{\phi}^{\mathsf{e}}_{ijk}(\eta_1, \eta_2, \eta_3) = \psi_i'(\eta_1)\phi_j(\eta_2)\phi_k(\eta_3)\boldsymbol{b}_1. \tag{2}$$

Notice that $\boldsymbol{\phi}^{\mathsf{e}}_{ijk} \cdot \boldsymbol{b}_2 = \boldsymbol{\phi}^{\mathsf{e}}_{ijk} \cdot \boldsymbol{b}_3 = 0$. Thus, the tangential component of $\boldsymbol{\phi}^{\mathsf{e}}_{ijk}$ vanishes along all edges not in the $\boldsymbol{b}_1$ direction. Consider the integral $a^{\mathsf{e}}_{lmn} := \int_{\mathcal{E}_{lmn}} \boldsymbol{\phi}^{\mathsf{e}}_{ijk} \cdot \boldsymbol{b}_1 \, dx$. Since $\phi_j(x_m) = \delta_{jm}$ and $\phi_k(x_n) = \delta_{kn}$, we find using (1) that

$$a^{\mathsf{e}}_{lmn} = \delta_{jm}\delta_{kn} \int_{x_l}^{x_{l+1}} \psi_i'(\eta_1) \, dx = \delta_{il}\delta_{jm}\delta_{kn}.$$

In other words, the integral of the tangential component of $\boldsymbol{\phi}^{\mathsf{e}}_{ijk}$ vanishes over all edges except for $\mathcal{E}_{ijk}$, for which this integral is 1. This feature ensures linear independence of the shape functions. Moreover, arguments similar to those in [7] can be used to show the finite element space is conforming in the space $H(\text{curl}; \hat{\Omega})$, where $\hat{\Omega} := (-1, 1)^3$. Using the curl-conserving transformation described in §3.9 of [6], the finite elements are also conforming in the space $H(\text{curl}; \Omega)$, where Ω is the domain of the higher-order finite element mesh.

2.2 Face Shape Functions

The vector field for a face-based finite element of degree p can be expressed in terms of the element coordinates as

$$\boldsymbol{u}^{\mathsf{f}}_p = u^{\mathsf{f}}_{1p}\boldsymbol{b}_1 + u^{\mathsf{f}}_{2p}\boldsymbol{b}_2 + u^{\mathsf{f}}_{3p}\boldsymbol{b}_3,$$

where $u^{\mathsf{f}}_{1p} \in Q_{p,p-1,p-1}$, $u^{\mathsf{f}}_{2p} \in Q_{p-1,p,p-1}$, and $u^{\mathsf{f}}_{3p} \in Q_{p-1,p-1,p}$ (again, see e.g. [7]).

Our present focus is on faces aligned with the $\boldsymbol{b}_3$ direction; similar constructions of shape functions hold for faces aligned with the other two directions. Let $\mathcal{F}_{ijk}$ denote the face with $\eta_1 \in (x_i, x_{i+1})$, $\eta_2 \in (x_j, x_{j+1})$, and $\eta_3 = x_k$. The shape function associated with this face is given by

$$\boldsymbol{\phi}^{\mathsf{f}}_{ijk}(\eta_1,\eta_2,\eta_3) = \psi'_i(\eta_1)\psi'_j(\eta_2)\phi_k(\eta_3)\boldsymbol{b}_3. \tag{3}$$

Notice that $\boldsymbol{\phi}^{\mathsf{f}}_{ijk}\cdot\boldsymbol{b}_1 = \boldsymbol{\phi}^{\mathsf{f}}_{ijk}\cdot\boldsymbol{b}_2 = 0$. Thus, the normal component of $\boldsymbol{\phi}^{\mathsf{f}}_{ijk}$ vanishes over all faces with normals not in the $\boldsymbol{b}_3$ direction. Next, consider the area integral $a^{\mathsf{f}}_{lmn} := \int_{\mathcal{F}_{lmn}} \boldsymbol{\phi}^{\mathsf{f}}_{ijk}\cdot\boldsymbol{b}_3\,dx$. Since $\phi_k(x_n) = \delta_{kn}$, we find using (1) that

$$\begin{aligned} a^{\mathsf{f}}_{lmn} &= \int_{\mathcal{F}_{lmk}} \delta_{kn}\psi'_i(\eta_1)\phi'_j(\eta_2)\,dx \\ &= \delta_{kn}\int_{x_l}^{x_{l+1}} \psi'_i(\eta_1)\,d\eta_1 \int_{x_m}^{x_{m+1}} \psi'_j(\eta_2)\,d\eta_2 = \delta_{il}\delta_{jm}\delta_{kn}. \end{aligned}$$

In other words, the integral of the normal component of $\boldsymbol{\phi}^{\mathsf{f}}_{ijk}$ vanishes over all faces except for $\mathcal{F}_{ijk}$, for which this integral is 1. Again, this ensures linear independence of the shape functions, and arguments similar to those in [7] can be used to show the finite element space is conforming in $H(\mathrm{div};\hat{\Omega})$. Using the divergence-conserving transformation described in §3.9 of [6], the finite elements are also conforming in the space $H(\mathrm{div};\Omega)$, where Ω is the domain of the higher-order finite element mesh.

2.3 Interior Shape Functions

The scalar field of an interior-based element is approximated by functions $u^{\mathsf{v}}_p \in Q_{p-1,p-1,p-1}$. Let V_{ijk} denote the cell with $\eta_1 \in (x_i, x_{i+1})$, $\eta_2 \in (x_j, x_{j+1})$, and $\eta_3 \in (x_k, x_{k+1})$. The shape function associated with this cell is given by

$$\phi^{\mathsf{v}}_{ijk}(\eta_1,\eta_2,\eta_3) = \psi'_i(\eta_1)\psi'_j(\eta_2)\psi'_k(\eta_3). \tag{4}$$

Consider the volume integrals $a^{\mathsf{v}}_{lmn} := \int_{V_{lmn}} \phi^{\mathsf{v}}_{ijk}\,dx$. We find using (1) that

$$a^{\mathsf{v}}_{lmn} = \int_{x_l}^{x_{l+1}} \psi'_i(\eta_1)\int_{x_m}^{x_{m+1}} \psi'_j(\eta_2)\int_{x_n}^{x_{n+1}} \psi'_k(\eta_3)\,dx = \delta_{il}\delta_{jm}\delta_{kn}.$$

In other words, the integral of ϕ^{v}_{ijk} vanishes over all regions except for V_{ijk}, for which this integral is 1. This ensures linear independence of the shape functions. Further, a polynomial function $u^{\mathsf{v}}_p \in Q_{p-1,p-1,p-1}$ can be expressed in terms of the shape functions as

$$u^{\mathsf{v}}_p = \sum_{i,j,k=0}^{p-1} c^{\mathsf{v}}_{ijk}\psi'_i(\eta_1)\psi'_j(\eta_2)\psi'_k(\eta_3), \qquad c^{\mathsf{v}}_{ijk}(u^{\mathsf{v}}_p) = \int_{V_{ijk}} u^{\mathsf{v}}_p\,dx.$$

Remark 1 Starting with the edge shape function $\boldsymbol{\phi}^{\mathsf{e}}_{ijk}$ in (2), notice that the face shape function $\boldsymbol{\phi}^{\mathsf{f}}_{ijk}$ in (3) is obtained simply by replacing $\phi_j(\eta_2)\boldsymbol{b}_1$ with $\psi'_j\boldsymbol{b}_3$. Likewise, ϕ^{v}_{ijk} in (4) is obtained from $\boldsymbol{\phi}^{\mathsf{f}}_{ijk}$ simply by replacing $\phi_k(\eta_3)\boldsymbol{b}_3$ with $\psi'_k(\eta_3)$.

2.4 Lowest-Order Shape Functions

The lowest-order counterparts of the one-dimensional higher-order shape functions $\phi_0, \ldots, \phi_p$ are piecewise linear and are denoted by $\phi_{0h}, \ldots \phi_{ph}$ (see Figure 2 (right) for the case of $p = 4$). Analogous to the the higher-order edge, face, and interior shape functions, we may define the lowest-order counterparts of (2), (3) and (4) as

$$\boldsymbol{\phi}^{\mathsf{e}}_{ijkh}(\eta_1, \eta_2, \eta_3) = \psi'_{ih}(\eta_1)\phi_{jh}(\eta_2)\phi_{kh}(\eta_3)\boldsymbol{b}_1, \tag{5}$$

$$\boldsymbol{\phi}^{\mathsf{f}}_{ijkh}(\eta_1, \eta_2, \eta_3) = \psi'_{ih}(\eta_1)\psi'_{jh}(\eta_2)\phi_{kh}(\eta_3)\boldsymbol{b}_3, \tag{6}$$

$$\phi^{\mathsf{v}}_{ijkh}(\eta_1, \eta_2, \eta_3) = \psi'_{ih}(\eta_1)\psi'_{jh}(\eta_2)\psi'_{kh}(\eta_3), \tag{7}$$

where ψ_{ih} is defined analogously to ψ_i as

$$\psi_{ih}(\eta_1) = \sum_{m=0}^{p} a_{im}\phi_{mh}(\eta_1).$$

By construction, the lowest-order edge, face, and interior shape functions in (5-7) have similar interpolatory properties to their higher-order counterparts. For example, the integrated tangential component of $\boldsymbol{\phi}^{\mathsf{e}}_{ijkh}$ is 1 along edge $\mathcal{E}_{ijk}$ and vanishes along all other edges of the GLL mesh just like the higher-order shape function $\boldsymbol{\phi}^{\mathsf{e}}_{ijk}$.

3 Spectral Equivalence Results

In this section, we summarize the spectral equivalence of mass and stiffness matrices of higher-order edge, face and interior-based elements with their assembled lowest-order counterparts on the GLL mesh. By spectral equivalence we mean that constants in the estimates are independent of the polynomial degree. In three dimensions, the constants for the equivalence are independent of element aspect ratios for mass matrices, while stiffness matrices have a weak dependence for edge-based elements but no dependence for face-based elements. More details, including proofs of the results, can be found in [4]. We use the notational convention $f \simeq g$ to mean that there exist positive constants c and C, independent of polynomial degree, such that $cg \leq f \leq Cg$ for non-negative scalars f and g.

3.1 Mass Matrix Equivalence

We follow closely in [4] the development given on pages 16 and 17 of [1] to show spectral equivalence of mass matrices. Based on these results, spectral equivalence for stiffness matrices is shown to follow.

Lemma 1 *Let $\boldsymbol{u}_h^{\mathsf{k}}$ denote the lowest-order interpolant of the higher-order vector function $\boldsymbol{u}_p^{\mathsf{k}}$, where $\mathsf{k} \in \{\mathsf{e}, \mathsf{f}\}$. Similarly, let u_h^{v} denote the lowest-order interpolant of the higher-order scalar function u_p^{v}. It holds that*

$$\|\boldsymbol{u}_h^{\mathsf{e}}\|_{L^2(\hat{\Omega})} \simeq \|\boldsymbol{u}_p^{\mathsf{e}}\|_{L^2(\hat{\Omega})}, \tag{8}$$

$$\|\boldsymbol{u}_h^{\mathsf{f}}\|_{L^2(\hat{\Omega})} \simeq \|\boldsymbol{u}_p^{\mathsf{f}}\|_{L^2(\hat{\Omega})}, \tag{9}$$

$$\|u_h^{\mathsf{v}}\|_{L^2(\hat{\Omega})} \simeq \|u_p^{\mathsf{v}}\|_{L^2(\hat{\Omega})}. \tag{10}$$

3.2 Stiffness Matrix Equivalence

The stiffness matrix for a higher-order edge-based element is associated with the curl semi-norm of $\boldsymbol{u}_p^{\mathsf{e}}$, which we denote by $|\nabla \times \boldsymbol{u}_p^{\mathsf{e}}|_{L^2(\hat{\Omega})}$. Similarly, the stiffness matrix for a higher-order face-based element is associated with the divergence semi-norm of $\boldsymbol{u}_p^{\mathsf{f}}$, which we denote by $|\nabla \cdot \boldsymbol{u}_p^{\mathsf{f}}|_{L^2(\hat{\Omega})}$.

Lemma 2 *Let $\boldsymbol{u}_h^{\mathsf{k}}$ denote the lowest-order interpolant of $\boldsymbol{u}_p^{\mathsf{k}}$, where $\mathsf{k} \in \{\mathsf{e}, \mathsf{f}\}$. It holds that*

$$|\nabla \times \boldsymbol{u}_h^{\mathsf{e}}|_{L^2(\hat{\Omega})} \simeq |\nabla \times \boldsymbol{u}_p^{\mathsf{e}}|_{L^2(\hat{\Omega})}, \tag{11}$$

$$|\nabla \cdot \boldsymbol{u}_h^{\mathsf{f}}|_{L^2(\hat{\Omega})} \simeq |\nabla \cdot \boldsymbol{u}_p^{\mathsf{f}}|_{L^2(\hat{\Omega})}. \tag{12}$$

4 Numerical Results

Numerical support for the estimates in (8-12) is provided in this section. For each of these estimates, we consider a generalized eigenvalue problem of the form $B_p x = \lambda B_h x$, where B_p and B_h are the higher- and lowest-order element mass or stiffness matrices corresponding to the estimate. Notice that B_p and B_h are singular for (11) and (12), with null spaces corresponding to gradients of node-based finite element functions and curls of edge-based finite element functions, respectively. For these two cases, we confirmed that the null spaces for B_p and B_h are identical. Further, the generalized eigenvalue problem was solved in a space orthogonal to the null space.

The smallest and largest eigenvalues corresponding to (8-10) are shown in Figure 3 (left) for elements in three dimensions. For completeness, results are also shown for node-based elements in the space H^1. Notice in all cases that the smallest and largest eigenvalues are bounded by those for node-based elements. This provides numerical support for (8-10) based on node-based spectral equivalence results in [1]. Similar results are shown in Figure 3 (right) which correspond to (11-12).

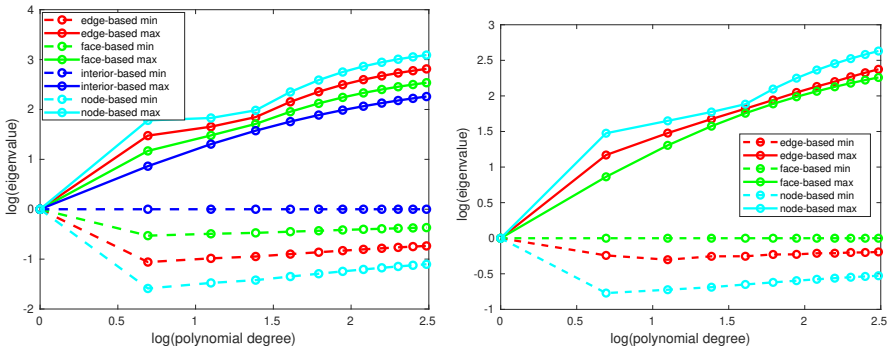

Fig. 3 Generalized eigenvalues associated with mass (left) and stiffness (right) matrices in three dimensions.

Acknowledgements Sandia National Laboratories is a multimission laboratory managed and operated by National Technology and Engineering Solutions of Sandia, LLC, a wholly owned subsidiary of Honeywell International Inc., for the U.S. Department of Energy's National Nuclear Security Administration under contract DE-NA0003525.

References

1. Claudio Canuto. Stabilization of spectral methods by finite element bubble functions. *Comput. Methods Appl. Mech. Engrg.*, 116:13–26, 1994.
2. Claudio Canuto, Paola Gervasio, and Alfio Quarteroni. Finite-element preconditioning of G-NI spectral methods. *SIAM J. Sci. Comput.*, 31(6):4422–4451, 2010.
3. Michel O. Deville and Ernest H. Mund. Chebyshev pseudospectral solution of second-order elliptic equations with finite element preconditioning. *J. Comput. Phys.*, 60(3):517–533, 1985.
4. Clark R. Dohrmann. Spectral equivalence properties of higher-order tensor product finite elements and applications to preconditioning. Technical Report SAND2021-0323, Sandia National Laboratories, 2021.
5. Marc Gerritsma. Edge functions for spectral element methods. In *Spectral and High Order Methods for Partial Differential Equations*, pages 199–207. Springer, 2011.
6. Peter Monk. *Finite Element Methods for Maxwell's Equations*. Oxford University Press, Oxford, 2003.
7. Jean-Claude Nédélec. Mixed finite elements in R^3. *Numer. Math.*, 35:315–341, 1980.
8. Deville Michel O. and Mund Ernest H. Finite-element preconditioning for pseudospectral solutions of elliptic problems. *SIAM J. Sci. Stat. Comput.*, 11(2):311–342, 1990.
9. Steven A. Orszag. Spectral methods for problems in complex geometry. *J. Comput. Phys.*, 37(1):70–92, 1980.
10. Andrea Toselli and Olof Widlund. *Domain Decomposition Methods - Algorithms and Theory*, volume 34 of *Springer Series in Computational Mathematics*. Springer-Verlag, Berlin Heidelberg New York, 2005.